Diffuse cosmic dipoles

Tiziana Trombetti*

INAF, Istituto di Radioastronomia
Via Piero Gobetti, 101, 40129 Bologna, Italy
**E-mail: trombetti@ira.inaf.it*

The boosting effects induced by the peculiar motion of an observer with respect to the Cosmic Microwave Background (CMB) rest frame can be explored to analyze the frequency dependence of the dipole. The improvements achievable with future CMB missions on our knowledge of CMB spectral distortions and Cosmic Infrared Background spectrum are discussed considering realistic uncertainties in relative calibration and foreground subtraction.

Keywords: CMB experiments, spectral distortions, reionization.

1. Introduction

The cosmic dipoles have a crucial relevance in cosmology since they are linked with the isotropy and homogeneity of the Universe at the largest scales. The observed dipole is a mixture of different contributions, including the observer motion with respect to the Cosmic Microwave Background (CMB) rest frame as well as dipoles from astrophysical (extragalactic and Galactic) sources. The CMB and Cosmic Infrared Background (CIB) spectra can be investigated by future anisotropy missions, as CORE[1] or LiteBIRD,[2] by exploring the frequency spectral behaviour of the dipole amplitude, thus without requiring an independent absolute calibration. Tiny CMB spectral distortions are predicted to be generated at different cosmic times in the evolving plasma. In the present work, I will focus on two well-defined types of signal, namely Bose-Einstein (BE) and Comptonization distortions. The precise interpretation of these signals could contribute to constraint primordial cosmological processes otherwise unexplored. The CIB spectrum amplitude and shape, still not well known, can provide a better understanding of the dust-obscured star-formation phase of galaxy evolution.

2. The CMB spectrum

One of the main features of the CMB is its frequency spectrum. To first approximation, it emerges from the thermalization epoch ($z \sim 10^6 - 10^7$) with a thermal black body (BB) shape owing to highly efficient interaction processes in the cosmic plasma, able to re-establish matter-radiation thermal equilibrium. Since COBE/FIRAS, no remarkable improvements have been achieved in the knowledge of CMB spectrum at $\nu \gtrsim 30$ GHz. Although gaining an absolute calibration precision of 0.57 mK, the FIRAS characterization of CIB amplitude and shape still presents a substantial uncertainty. To overcome the absolute calibration problem, it is possible to investigate the CMB and CIB spectra by looking at the frequency spectral behaviours of their dipole amplitude thanks to future CMB missions, as e.g.

CORE. The CMB spectrum can set constraints on various types of non-standard processes, including non evaporating BH spin, small scale magnetic fields power spectra, vacuum energy density and particle decay.

2.1. *Spectral distortions*

Different energy injections in the radiation field due to fundamental unavoidable processes occurring at different cosmic times cause the departure of CMB spectrum from a perfect BB.

At early times, a BE-like distorted spectrum with a positive (dimensionless) chemical potential is produced by the dissipation of primordial perturbations at small scales,[3] damped by photon diffusion and non-linear processes and then invisible in CMB anisotropies.[4] Moreover, because of the matter temperature faster decrease with respect to that of radiation temperature in an expanding Universe, colder electrons induce Bose condensation of CMB photons, mainly resulting into a BE-like distortion with negative chemical potential. The photon occupation number of the BE spectrum is $\eta_{BE} = 1/(e^{x_e+\mu} - 1)$, where μ is the chemical potential that quantifies the fractional energy, $\Delta\varepsilon/\varepsilon_i$, exchanged in the plasma during the interaction, $x_e = x/\phi(z)$, $\phi(z) = T_e(z)/T_{CMB}(z)$, being $T_e(z)$ the electron temperature, $T_{CMB} = T_0(1+z)$, T_0 the present CMB temperature in the BB approximation and $x = h\nu/kT_{CMB}$ a redshift independent, dimensionless frequency. For small distortions, $\mu \simeq 1.4\Delta\varepsilon/\varepsilon_i$ and $\phi_{BE} \simeq (1 - 1.11\mu)^{-1/4}$.[a]

Cosmological reionization associated with the early stages of structure and star formation induces electron heating that is responsible for late type distortions, described, at high frequency,[b] by a Comptonization spectrum.[7] It is quantified by the Comptonization parameter $u(t) = \int_{t_i}^{t}[(\phi - \phi_i)/\phi](k_B T_e/m_e c^2) n_e \sigma_T c dt$. For small energy injections and integrating over the relevant epochs $u \simeq (1/4)\Delta\varepsilon/\varepsilon_i$.

3. Future CMB missions

Among the many different classes of CMB missions, here I will focus on three recent proposals with concepts and designs aimed at improving the measure of polarization anisotropies and at minimizing the impact of foregrounds on CMB maps using a large number of frequency channels, with relevant outcomes for e.g. our knowledge of the reionization process and the primordial background of gravitational waves.

The Primordial Inflation Explorer[8] (PIXIE) is an Explorer-class mission submitted to NASA in 2011 aimed at mapping the CMB and the diffuse astrophysical foregrounds over the full sky, from 30 GHz to 6 THz (1 cm to 50 μm) with degree

[a] At decreasing frequencies, photon emission processes produce a frequency dependent, decreasing chemical potential and the convergency to a blackbody at matter temperature at extremely low frequencies.[5] For positive (negative) μ they imply a minimum (maximum) in the brightness temperature, as well as the avoiding of the divergency of the BE spectrum for negative μ.
[b] Associated free-free distortions are instead relevant at low frequencies.[6]

resolution and high signal to noise ratio in absolute intensity and linear polarization. It is designed to perform absolute spectroscopy measurements and to simultaneously observe the large-scale CMB B-modes. It will provide crucial constraints on Universe ionization history, on CIB spectrum and anisotropies. Indeed, PIXIE will trace CIB monopole, dipole and higher order power spectrum up to $z \sim 3$ for matter distribution analyses. The cross correlation of temperature and polarization anisotropies will produce more stringent constraints on the optical depth parameter, the gas temperature and the Universe reionization at $z \sim 10$. Great hopes on CMB spectral distortion parameters are expected from PIXIE, thanks to its absolute calibration of the CMB temperature measure with a precision about 10^3 times better than FIRAS.

LiteBIRD is a Lite (Light) Satellite for the studies of B-mode polarization and Inflation from cosmic background Radiation Detection at the extremely early Universe proposed to JAXA in February 2015. It is a highly-targeted, low-cost Japanese B-mode mission concept, aimed at the B-modes detection at the level of $r \sim 10^{-3}$, its main scientific goal being one order of magnitude better than what can be done from the ground. Its primary strategy is the focus on r measurement in synergy with ground based super telescopes which are necessary for an accurate subtraction of the lensing contribution to B-mode.

Cosmic ORigins Explorer (CORE), submitted to the European Space Agency (ESA) in October 2016 in response to a call for future medium-sized space mission proposals for the M5 launch opportunity of ESAs Cosmic Vision programme, is a satellite dedicated to microwave polarization. CORE is targeted to provide and exploit definitive maps of CMB polarization anisotropies at large and medium angular scales, with a suppression of all systematic effects at an extreme accuracy level. The instrument will host about 19 frequency channels over a range spanning the 60–600 GHz interval, in order to control astrophysical foreground emissions.

4. CMB and CIB dipoles

A relative velocity between an observer and the CMB rest frame induces a dipole in the observed CMB sky temperature through the Doppler effect. This dipole, the so called $\ell = 1$ anisotropy, is likely dominated by the velocity of the Solar System, $\vec{\beta_S} = \vec{v_S}/\vec{c}$, with respect to the CMB (Solar dipole), with a seasonal modulation due to the velocity of the Earth or the satellite, $\vec{\beta_o}$, with respect to the Sun (orbital dipole).

In addition, an intrinsic dipole is induced by the Sachs-Wolfe effect at the last-scattering surface and by a large-scale dipolar Newtonian potential.[9] In a ΛCDM cosmology, this dipole should be of order of the Sachs-Wolfe plateau amplitude (10^{-5}), but it could be larger in the case of more exotic models. Neglecting the orbital dipole (useful for calibration aims), and denoting with $\vec{\beta}$ the relative velocity of the Solar dipole, it is possible to forecast the CORE improvements in the dipole recovery including also potential foreground and calibration residuals.[10] The

dipole amplitude is directly proportional to the first (logarithmic) derivative with respect to the frequency of the photon occupation number, $\eta(\nu)$, which is related to the thermodynamic temperature, $T_{therm}(\nu)$, defined as the temperature of the blackbody having the same $\eta(\nu)$ at the frequency ν, by:

$$T_{therm} = \frac{h\nu}{k_B \ln(1 + 1/\eta(\nu))}. \tag{1}$$

Differencing the measure of T_{therm} in the direction of motion and in its perpendicular direction one gets:[11]

$$\Delta T_{therm} = \frac{h\nu}{k_B} \left\{ \frac{1}{\ln[1 + 1/\eta(\nu)]} - \frac{1}{\ln[1 + 1/\eta(\nu(1+\beta))]} \right\}. \tag{2}$$

To first order in β, ΔT_{therm} is approximated by:

$$\Delta T_{therm} \simeq -\frac{x\beta T_0}{(1+\eta)\ln^2(1 + 1/\eta)} \frac{d\ln\eta}{d\ln x}. \tag{3}$$

A direct determination of the CIB spectral shape is not trivial since it requires absolute intensity measurements and it is also limited by foreground signal, that, in the case of Galactic emission, has a similar shape. Even though the dipole amplitude is about 10^{-3} of the monopole, its spatial distribution is known, hence, an indirect approach may provide in the future a robust measurement of the CIB. The analytic form of the CIB spectrum, observed at present time, is:[12]

$$\eta_{CIB} = \frac{c^2}{2h\nu^3} I_{CIB}(\nu) = I_0 \left(\frac{k_B T_{CIB}}{h\nu_0} \right)^{k_F} \frac{x_{CIB}^{k_F}}{e^{x_{CIB}} - 1}, \tag{4}$$

with $T_{CIB} = (18.5 \pm 1.2)$ K, $x_{CIB} = h\nu/k_B T_{CIB} = 7.78(\nu/\nu_0)$, $\nu_0 = 3 \times 10^{12}$ Hz and $k_F = 0.64 \pm 0.12$. Here I_0 sets the CIB spectrum amplitude, its best-fit value being $(1.3 \pm 0.4) \times 10^{-5}$. The CIB dipole should be detectable by CORE in its highest frequency bands. Defining the motion vector of the observer, from the dipole direction of the *Planck* 2015 release, I produced the maps at a given observational frequency, ν_{obs}, from the photon distribution function, $\eta_{BB,dist}$, for the assumed type of spectra (BB, CIB, BE or Comptonization (C)) at the frequency ν_{obs} multiplied by $(1 - \hat{n} \cdot \vec{\beta})/(1 - \beta^2)^{1/2}$ to account for all the possible sky directions with respect to the observer peculiar velocity. The observed signal map in thermodynamic temperature is a generalization of Eq. (1):

$$T_{therm}^{BB/dist}(\nu, \hat{n}, \vec{\beta}) = \frac{xT_0}{\ln(1/(\eta(\nu, \hat{n}, \vec{\beta})^{BB/dist} + 1))}, \tag{5}$$

where $\eta(\nu, \hat{n}, \vec{\beta}) = \eta(\nu')$ with $\nu' = \nu((1 - \hat{n} \cdot \vec{\beta})/(1 - \beta^2)^{1/2}$. Decomposing the maps into spherical harmonics and reproducing them from the $a_{\ell m}$ up to a desired multipole ℓ_{max}, I derived the expected signal (see Fig. 1) finding that it is important for the dipole, can be considerable for the quadrupole and, depending on the distortion parameters, still not negligible for the octupole (although depending on the amplitude relative to experimental noise levels). For higher-order multipoles, the signal is essentially negligible.

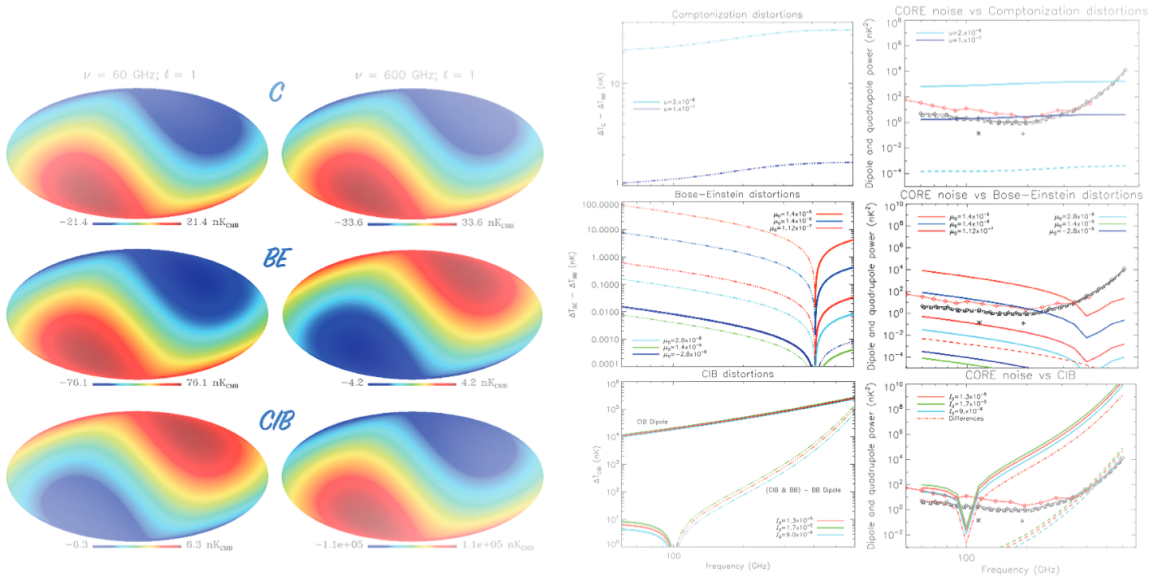


Fig. 1. Left: typical maps of dipole pattern (after the subtraction of the CMB blackbody dipole) for the three considered types of signal. Middle: dipole frequency behaviour. Right: angular power spectrum of the maps of dipole pattern compared with the sensitivity (diamonds) of CORE (black) and LiteBIRD (red). The quadrupole signal (dashes) is also shown in one case of BE distortion and in the case of CIB. See also the legend and the text. A dapted from Ref. 10 [©SISSA Medialab Srl. Reproduced by permission of IOP Publishing. All rights reserved].

5. Results and Conclusions

To recover the dipole parameters (amplitude and direction) it is essential to perform Markov Chain Monte Carlo (MCMC) analyses. I assumed the *Planck* common mask 76 (in temperature), publicly available from the *Planck* Legacy Archive (PLA),[13] exploiting its extension that excludes all the pixels at $|b| \leq 30°$. I first explored the dipole reconstruction ability for different frequency channels and then the implications for CMB spectral distortions and CIB starting from the ideal case (i.e., without calibration errors or sky residuals). The dipole can be parametrized as $d(\hat{n}) = A\hat{n} \cdot \hat{n}_0 + T_0$, where $\hat{n}$ and $\hat{n}_0$ are the unit vectors defined respectively by the Galactic longitudes and latitudes (l, b) and (l_0, b_0). The dipole map used in the simulations was generated assuming the measured dipole amplitude best-fit values, $A = (3.3645 \pm 0.002)$ mK, and direction, $l_0 = 264.00 \pm 0.03$ and $b_0 = 48.24 \pm 0.02$, as found in *Planck* 2015 release.[14]

To quantify the ideal CORE sensitivity to spectral distortion parameters and CIB amplitude, I carried out detailed simulations assuming a certain model and quantifying the accuracy level at which (in the presence of noise and of potential residuals) the key parameters can be recovered. I consider twelve, physically or observationally motivated, reference cases, from a (reference) blackbody spectrum, a CIB spectrum at the FIRAS best-fit amplitude, BE and C spectra with different μ_0 and u values. For each model I generate an ideal sky (the prediction) and a sky with white Gaussian noise realizations (simulated data). I calculated $\Delta\chi^2$ to quantify the significance level at which each model can be potentially detected or

ruled out. I consider three approaches: (a) analyzing each of the 19 frequency channels (assumed independent from each other); (b) using the 171 (19 ·18/2) combinations of the maps differences from pairs of frequency bands; (c) combining (a) and (b).

Approach (a) compares the dipole amplitude of a distorted spectrum with that of the blackbody, being sensitive to the overall difference between the two cases, while approach (b) compares the dipole signal at different frequencies for each type of spectrum, being so sensitive to its slope. The significance of the CIB amplitude recovery is increased in case b), because of the very steep frequency shape of its dipole spectrum. In general, this does not occur for CMB distortion parameters, and, in particular, approach (b) can make the recovery of the Comptonization distortion more difficult. Method c) typically results in an overall advantage. Including potential residuals from imperfect foreground subtraction and calibration (characterized by effective parameters $E_{\rm cal}$ and $E_{\rm for}$) may affect these results, but still the improvement for I_0^{CIB} ranges from a factor of 4 (a) to a factor of about 15 or 20 for (b) and (c), respectively. The recovery of CMB spectral distortion parameters is also very promising. Including the extended mask in case c), I find a significant improvement with respect to the full sky: the significance of the CIB amplitude recovery improves by about 50% and that on the BE distortion by about 20%, indicating the relevance of optimising the selection of the sky region. Tab. 1 summarizes the main results expressed in terms of a factor characterizing the improvement with respect to FIRAS.

Table 1. Predicted improvement in the recovery of the distortion parameters with respect to FIRAS for different calibration and foreground residual assumptions. "P06" stands for the *P*lanck common mask, while "P06ext" is the extended P06 mask. When not stated, all values refer to $E_{\rm cal}$ and $E_{\rm for}$ at $N_{\rm side} = 64$. From Ref. 10 [©SISSA Medialab Srl. Reproduced by permission of IOP Publishing. All rights reserved].

	$E_{\rm cal}$ (%)	$E_{\rm for}$ (%)	CIB amplitude	BE	C
Ideal case, all sky	-	-	$\simeq 4.4 \times 10^3$	$\simeq 10^3$	$\simeq 6.0 \times 10^2$
All sky	10^{-4}	10^{-2}	$\simeq 15$	$\simeq 42$	$\simeq 18$
P76	10^{-4}	10^{-2}	$\simeq 19$	$\simeq 42$	$\simeq 18$
P76ext	10^{-2}	10^{-2}	$\simeq 17$	~ 4	~ 2
P76ext	10^{-4}	10^{-2}	$\simeq 22$	$\simeq 47$	$\simeq 21$
P76ext	10^{-4}	10^{-3}	$\simeq 2.1 \times 10^2$	$\simeq 2.4 \times 10^2$	$\simeq 1.1 \times 10^2$
P76ext	$10^{-3}_{(\leq 295)}$–$10^{-2}_{(\geq 340)}$	10^{-2}	$\simeq 19$	$\simeq 26$	$\simeq 11$
P76ext	$10^{-3}_{(\leq 295)}$–$10^{-2}_{(\geq 340)}$	10^{-3}	$\simeq 48$	$\simeq 35$	$\simeq 15$
P76ext, $N_{\rm s} = 128$	$10^{-3}_{(\leq 295)}$–$10^{-2}_{(\geq 340)}$	10^{-2}	$\simeq 38$	$\simeq 51$	$\simeq 23$
P76ext, $N_{\rm s} = 128$	$10^{-3}_{(\leq 295)}$–$10^{-2}_{(\geq 340)}$	10^{-3}	$\simeq 43$	$\simeq 87$	$\simeq 39$
P76ext, $N_{\rm s} = 256$	$10^{-3}_{(\leq 295)}$–$10^{-2}_{(\geq 340)}$	10^{-2}	$\simeq 76$	$\simeq 98$	$\simeq 44$
P76ext, $N_{\rm s} = 256$	$10^{-3}_{(\leq 295)}$–$10^{-2}_{(\geq 340)}$	10^{-3}	$\simeq 85$	$\simeq 1.6 \times 10^2$	$\simeq 73$

Acknowledgments

I acknowledge partial supports from the INAF PRIN SKA/CTA project FORECaST, from ASI/INAF agreement n. 2014-024-R.1 for the *Planck* LFI Activity of Phase E2 and from the ASI/Physics Department of the University of Roma–Tor Vergata agreement n. 2016-24-H.0 for study activities of the Italian cosmology community. It is a pleasure to thank the many colleagues of the *Planck* and CORE collaborations for constructive discussions. Some of the results in this paper have been derived using the HEALPix[15] package.

References

1. Delabrouille, J., de Bernardis, P., Bouchet, F. R., et al. 2018, JCAP, 4, 014
2. Ishino, H., Akiba, Y., Arnold, K., et al. 2016, Proc. SPIE, 9904, 99040X
3. Hu, W., Scott, D., & Silk, J. 1994, ApJL, 430, L5
4. Chluba, J., & Sunyaev, R. A. 2012, MNRAS, 419, 1294
5. Danese, L., & de Zotti, G. 1982, A&A, 107, 39
6. Trombetti, T., & Burigana, C. 2014, MNRAS, 437, 2507
7. Ya. B. Zel'dovich, A.F. Illarionov, R.A. Syunyaev, JETP, 1972, Vol. 35, No. 4, p. 643
8. Kogut, A., Fixsen, D. J., Chuss, D. T., et al. 2011, JCAP, 7, 025
9. Roldan, O., Notari, A., & Quartin, M. 2016, *JCAP*, 6, 026
10. Burigana, C., Carvalho, C. S., Trombetti, T., et al. 2018, JCAP, 4, 021
11. Danese, L., & de Zotti, G. 1981, A&A, 94, L33
12. Fixsen, D. J., Dwek, E., Mather, J. C., Bennett, C. L., & Shafer, R. A. 1998, ApJ, 508, 123
13. Planck 2015 Release Explanatory Supplement, `https://www.cosmos.esa.int/documents/387566/387639/Planck_2015_results_explanatory_supplement.pdf/8b18ecea-49b2-45fa-89e4-9b74e9fb051b`
14. Planck Collaboration, Adam, R., Ade, P. A. R., et al. 2016, *A&A*, 594, A1
15. Górski, K. M., Hivon, E., Banday, A. J., et al. 2005, ApJ, 622, 759